

Supplement of Biogeosciences, 13, 2257–2277, 2016  
<http://www.biogeosciences.net/13/2257/2016/>  
doi:10.5194/bg-13-2257-2016-supplement  
© Author(s) 2016. CC Attribution 3.0 License.



Biogeosciences  Open Access

*Supplement of*

## **Molecular characterization of dissolved organic matter from subtropical wetlands: a comparative study through the analysis of optical properties, NMR and FTICR/MS**

**Norbert Hertkorn et al.**

*Correspondence to:* Rudolf Jaffé ([jaffer@fiu.edu](mailto:jaffer@fiu.edu))

The copyright of individual parts of the supplement might differ from the CC-BY 3.0 licence.

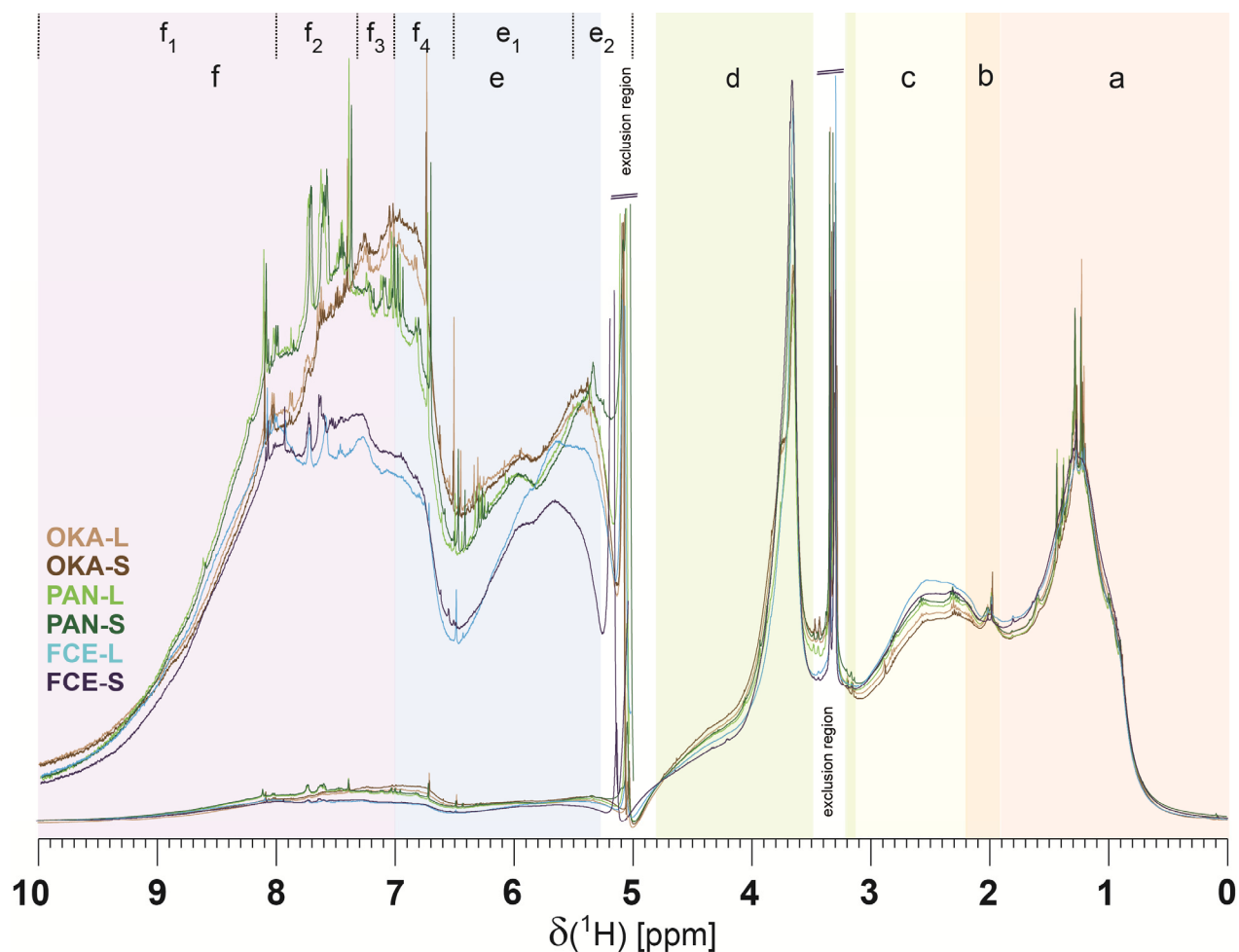


**Figure S1.**  $^1\text{H}$  NMR spectra of six wetland SPE-DOM ( $\text{CD}_3\text{OD}$ ; 500 MHz), acquired with solvent suppression and exclusion regions used in the computation of NMR section integrals and overlay NMR spectra (Fig. 2 and this figure) which denote  $\text{HD}_2\text{COD}$  and residual  $\text{HDO}$ , with section of unsaturated protons ( $\delta_{\text{H}} > 5$  ppm) vertically expanded. Intensities are normalized to 100% total integral in the entire chemical shift range shown ( $\delta_{\text{H}} = 0 \dots 10$  ppm). Fundamental substructures are indicated from higher to lower field (from right to left), (a) aliphatics,  $\underline{\text{H}}\text{CCC}$ ; (b) “acetate-analogue”,  $\underline{\text{H}}_3\text{CC}(=\text{O})\text{-O-}$ ; (c) carboxyl-rich alicyclic materials (CRAM),  $\underline{\text{H}}\text{C}(\text{C})\text{-COX}$ ; (d) “carbohydrate-like” and methoxy,  $\underline{\text{H}}\text{CO}$ ; (e) olefinic,  $\underline{\text{H}}\text{C}=\text{C}$ ; and (f) aromatic NMR resonances  $\underline{\text{H}}\text{C}_{\text{ar}}$  (cf. text). Further division of unsaturated protons provided (f<sub>1</sub>) polycyclic and polycarboxylated aromatics as well as six-membered nitrogen heterocycles ( $\delta_{\text{H}} > 8$  ppm); (f<sub>2</sub>) electron withdrawing substituents (COX; Perdue et al., 2007;  $\delta_{\text{H}} \approx 7.3 - 8.0$  ppm); (f<sub>3</sub>) electroneutral substituents (alkyl, H, R;  $\delta_{\text{H}} \approx 7.0 - 7.3$  ppm); (f<sub>4</sub>) electron-donating substituents (OR, OH, phenolics;  $\delta_{\text{H}} \approx 6.5 - 7.0$  ppm); (e<sub>1</sub>) polarized and conjugated olefins; ( $\delta_{\text{H}} \approx 5.5 - 6.5$  ppm); (e<sub>2</sub>) isolated olefins ( $\delta_{\text{H}} \approx 5.0 - 5.5$  ppm), with conceivable contributions from anomeric protons and ester groups (cf. discussion of 2D NMR spectra).

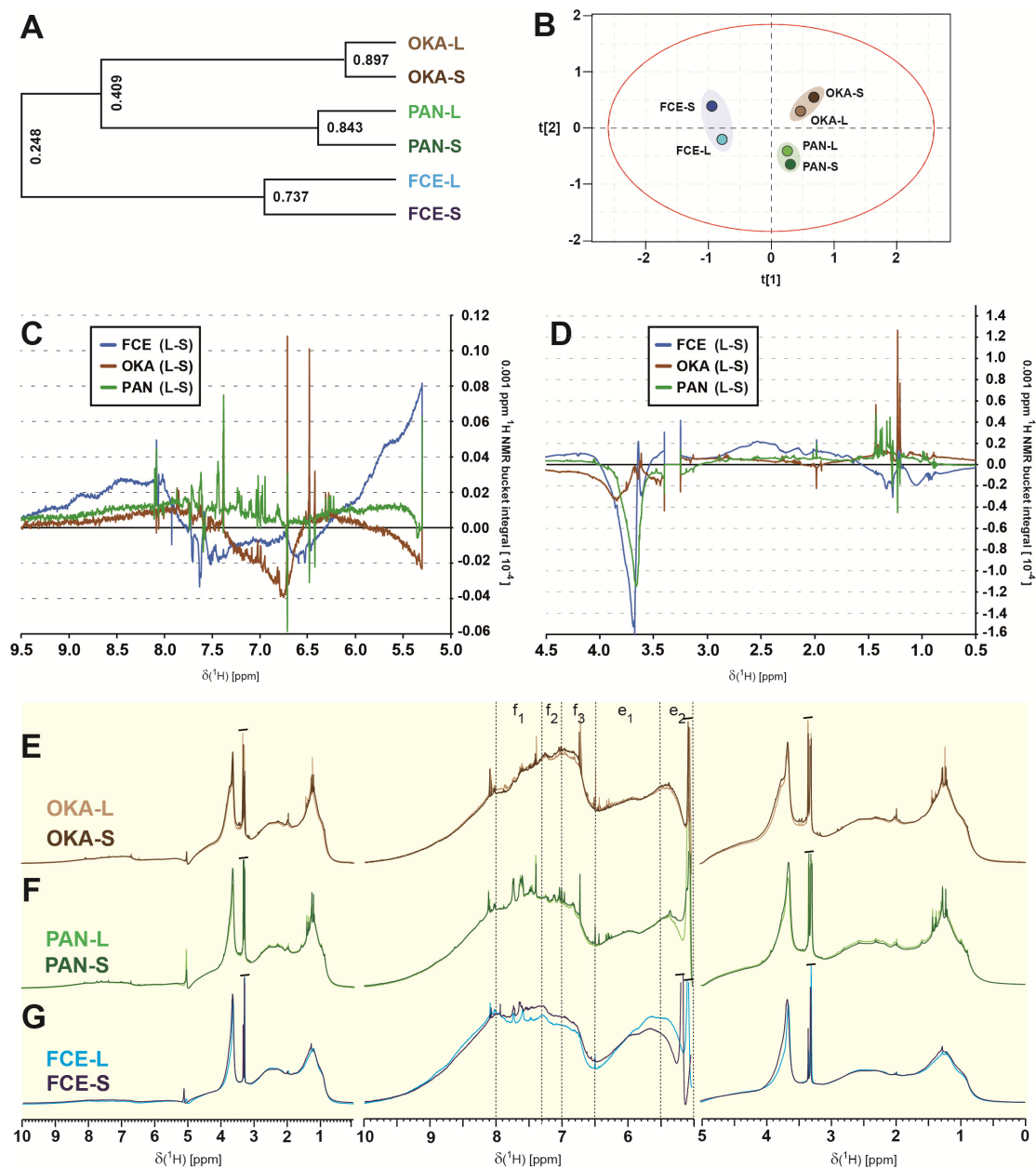


**Figure S2.**  $^1\text{H}$  NMR spectra of wetland SPE-DOM ( $\text{CD}_3\text{OD}$ ; 500 MHz). Similarity assessment by means of (panel A) hierarchical cluster analysis (Pearson) and (panel B) PCA as well as (panels C, D) computed difference  $^1\text{H}$  NMR spectra of 3 wetland SPE-DOM pairs (L-S: long minus short hydroperiod) as derived from 0.001 ppm buckets in area-normalized  $^1\text{H}$  NMR spectra; used chemical shift range:  $\delta_{\text{H}} = 9.5 - 0.5$  ppm, with exclusion of residual water and methanol NMR resonances. Panels E, F, G: Manual overlay according to identical  $^1\text{H}$  NMR section integral in the respective regions of  $^1\text{H}$  NMR chemical shift shown: (left column) entire NMR spectrum ( $\delta_{\text{H}} = 0 - 10$  ppm); (center column) section of unsaturated protons ( $\delta_{\text{H}} = 5 - 10$  ppm); (right column) section of aliphatic protons ( $\delta_{\text{H}} = 0 - 5$  ppm). Panel E: OKA; panel F: PAN, and panel G: FCE SPE-DOM. Sections  $f_n$  of unsaturated protons are denoted as provided in Fig. S1.

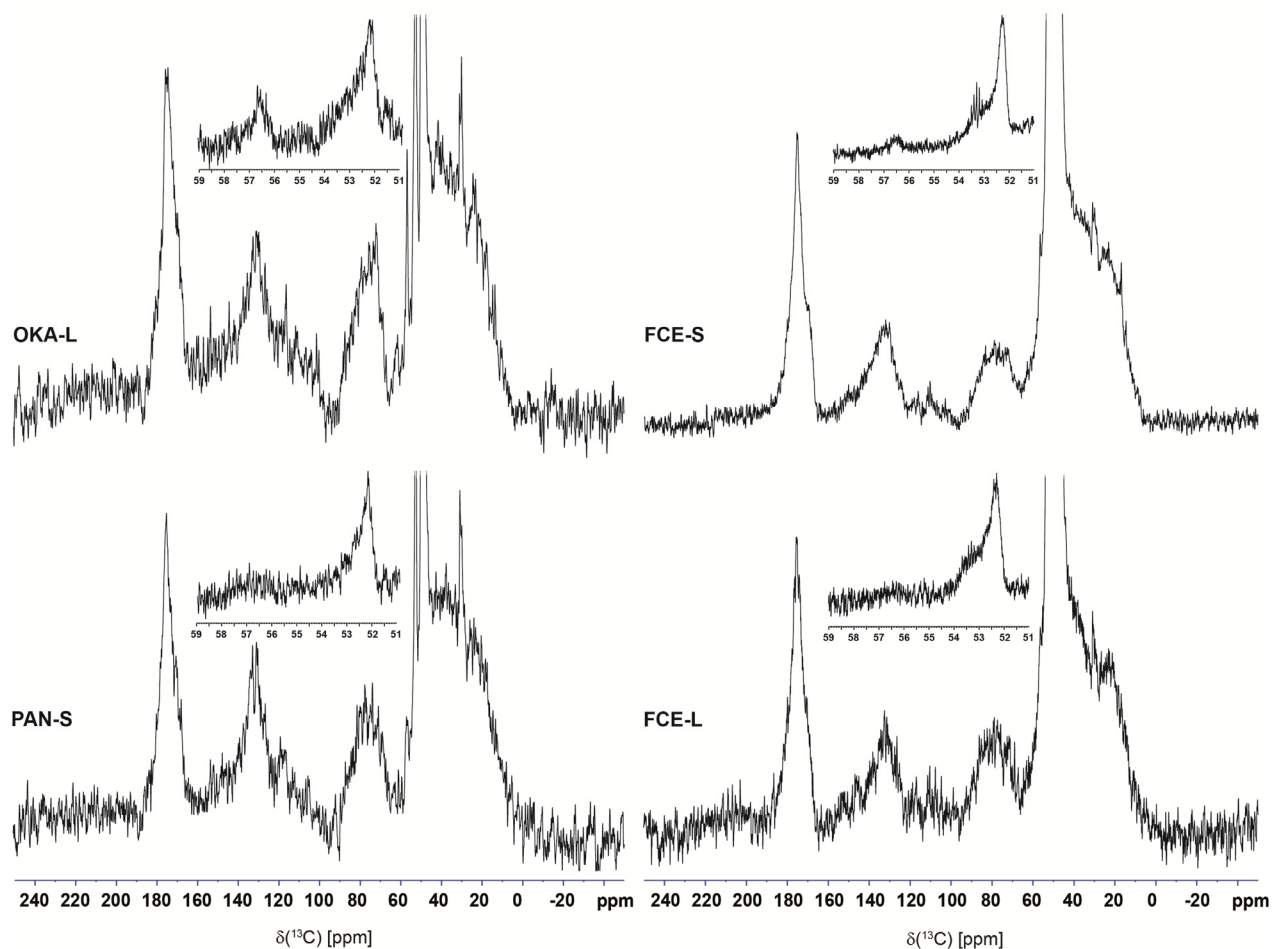


**Figure S3.**  $^{13}\text{C}$  NMR spectra of selected wetland SPE-DOM; full spectra computed with 35 Hz exponential line broadening; insert: section of methoxy peaks ( $\delta_{\text{C}} = 51\text{-}59$  ppm; computed with 2 Hz line broadening); OKA-L and PAN-S: in  $^{12}\text{CD}_3\text{OD}$  at  $B_0 = 11.7$  T; FCE in  $\text{CD}_3\text{OD}$  at  $B_0 = 18.8$  T.

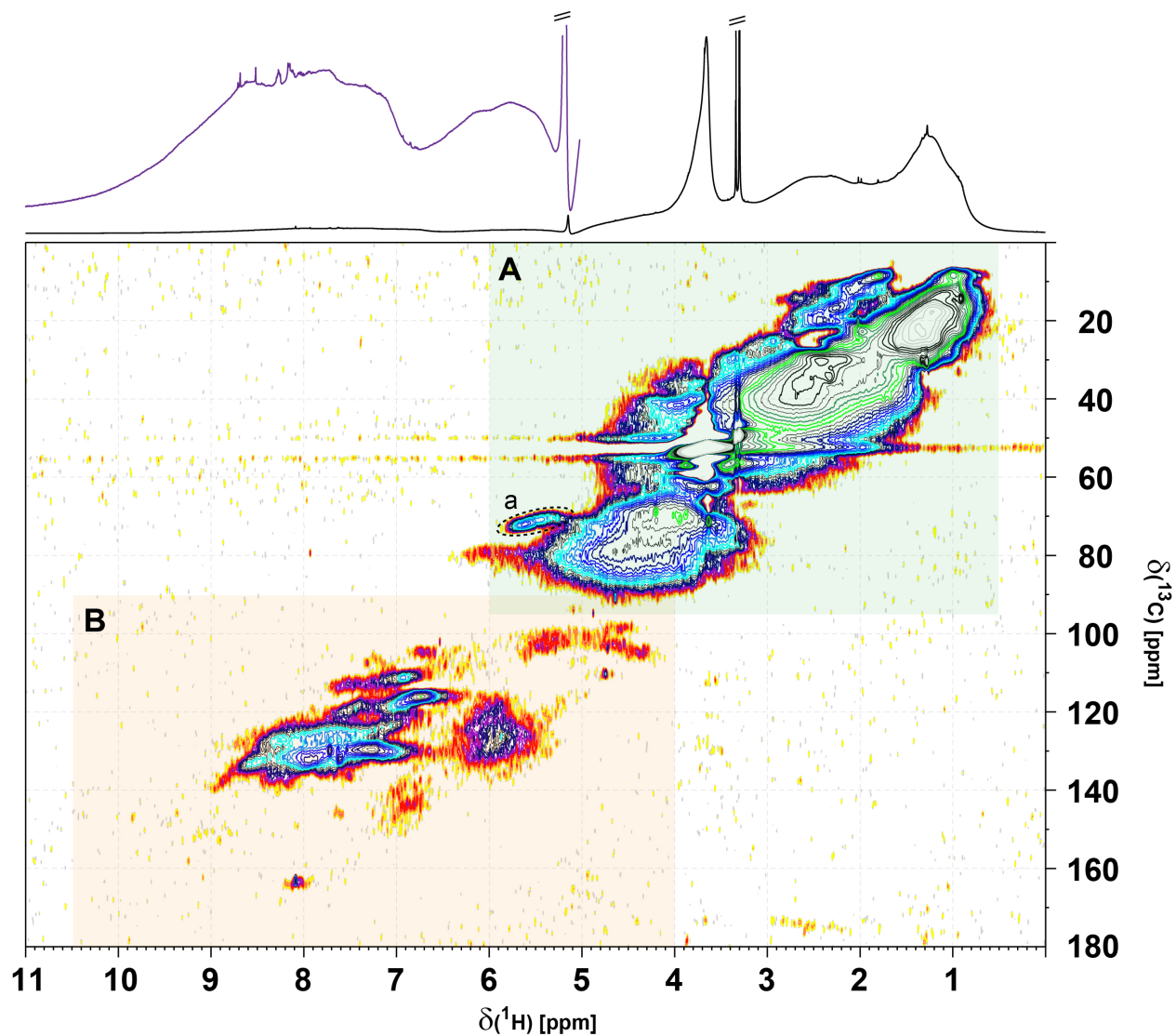


**Figure S4.**  $^1\text{H}$ ,  $^{13}\text{C}$  HSQC NMR spectrum of SPE-DOM FCE-S, with regions shown in figures: (A) chemical environments of  $\text{sp}^3$ -hybridized carbon (aliphatic  $\text{CH}_n$  units; Fig. 5); (B) chemical environments of  $\text{sp}^2$ -hybridized carbon (unsaturated, i. e. olefinic and aromatic CH units; Fig. 4). Sensitivity enhanced apodization is used to emphasize less abundant  $\text{sp}^2$ -hybridized carbon (overall HSQC cross peak integral <4% of aliphatic units) environments at the cost of resolution in case of aliphatic  $\text{CH}_n$  units ( $n = 1 - 3$ ).

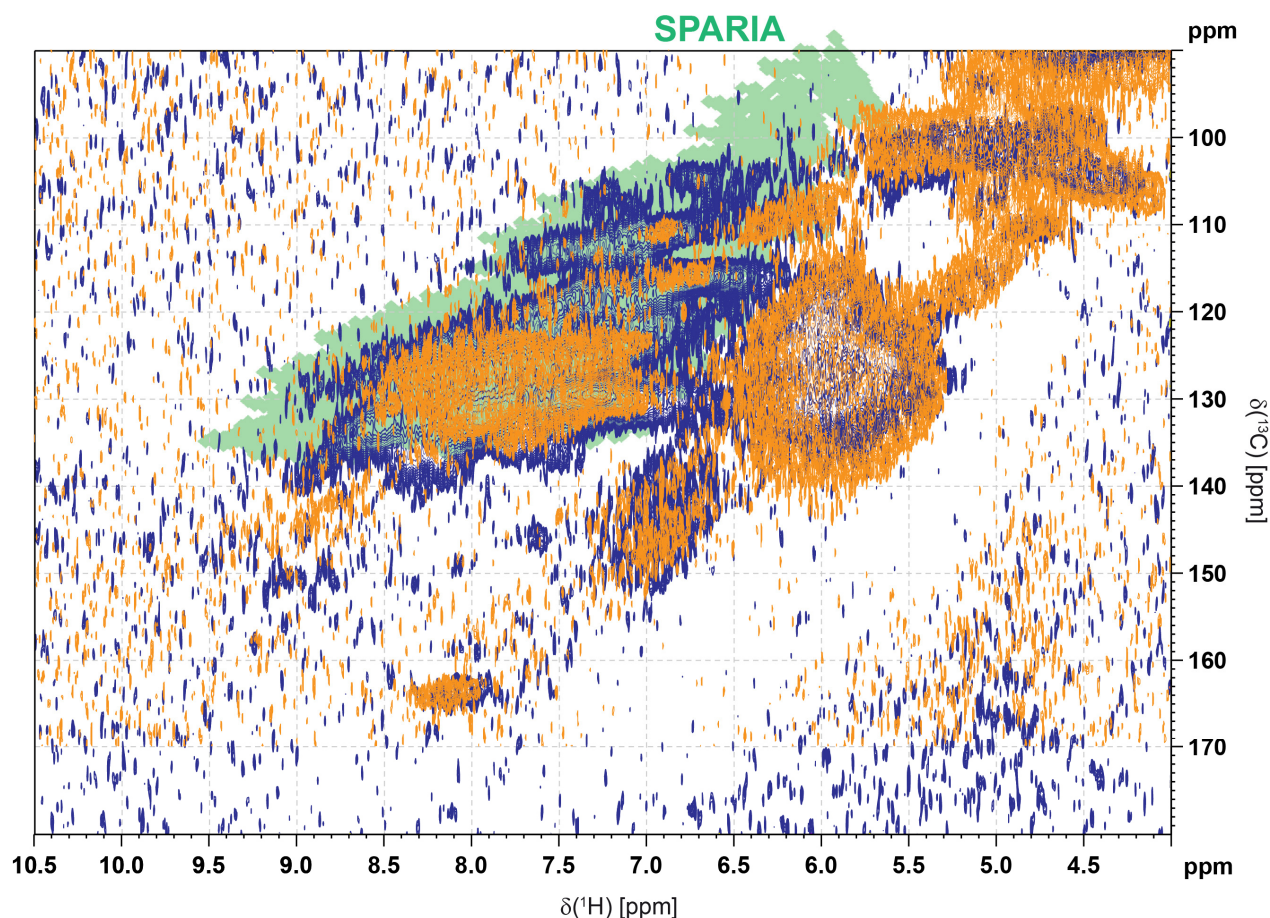


**Figure S5.** Overlay of  $^1\text{H}$ ,  $^{13}\text{C}$  HSQC NMR spectra of SPE-DOM FCE-S (dark blue) and South Atlantic SPE-DOM at fluorescence maximum (48 mg, FMAX; orange: Hertkorn et al., 2013), together with region of HSQC NMR cross peaks accessible for single aromatic rings with full range of electron-withdrawing (COX), electroneutral (R, H) and electron donating substitution (OH, OR), shown in green color (SPARIA: Perdue et al., 2007). Wetland SPE-DOM shows more exhaustive coverage of single aromatic rings from contributions of multiply oxygenated aromatics ( $\delta_{\text{H}} < 7$  ppm;  $\delta_{\text{C}} < 120$  ppm), likely originating from plant phenolics but also from polycarboxylated aromatics and PAH derivatives ( $\delta_{\text{H}} > 8.5$  ppm). In contrast, open ocean SPE-DOM FMAX exhibits a larger abundance as well as overall chemical diversity of  $\alpha,\beta$  unsaturated and C-conjugated olefins, likely originating from marine natural products; for assignment of HSQC cross peaks, see Figs. 4 and 5, and Hertkorn et al., 2013.

*Comparison of wetland SPE-DOM FCE-L with a South Atlantic open ocean SPE-DOM:*

Wetland SPE-DOM FCE-S, which showed the most conspicuous signature of  $\text{C}_{\text{sp}^2}\text{H}$  HSQC cross peaks (Fig. 4) of all wetland DOM was compared with Atlantic open ocean SPE-DOM MAX obtained at 48 m depth where the fluorescence maximum was located, supposedly corresponding to maximum biological activity at this open ocean location (Hertkorn et al., 2013). The overall envelope of  $\text{C}_{\text{sp}^3}\text{H}$  aliphatic HSQC cross peaks ( $\delta_{\text{H}} \sim 1\text{-}5$  ppm) of South Atlantic FMAX SPE-DOM (at 48 m depth) reached out to larger  $^{13}\text{C}$  NMR chemical shift values by  $\sim 7$  ppm on

average (Fig. 13b in Hertkorn et al., 2013), suggesting increased extent of (remote) aliphatic branching in marine SPE-DOM compared with wetland SPE-DOM. In contrast, HSQC cross peaks of methyl groups terminating extended aliphatic systems ( $\text{H}_3\text{C}-\text{C}_n-\text{Z}$ ;  $n \geq 2$ ; Z: any heteroatom; section a; Fig. 5) occupied a larger area in FCE-S than in marine SPE-DOM FMAX, and extended down to  $\delta_{\text{C}} \sim 32$  ppm at  $\delta_{\text{H}} \sim 0.9 - 1.2$  ppm. The abundance and chemical diversity of methyl bound to olefins ( $\text{C}=\text{CCH}_3$  groups and, possibly,  $\text{SCH}_3$  groups, section b; Fig. 5) was also larger in wetland SPE-DOM FCE-L than in marine SPE-DOM FMAX. Similarly, the methylene HSQC cross peak associated with  $\text{C}-\text{CH}_2-\text{COOH}$  groups in SPE-DOM FCE-L (section e; Fig. 5) extended downfield to  $\delta_{\text{H}} > 3.5$  ppm, approx. 0.4 ppm further downfield than that of SPE-DOM FMAX (Fig. 8b; Hertkorn et al., 2013). The chemical diversity of methoxy groups ( $\text{OCH}_3$ ) in wetland SPE-DOM FCE-L substantially exceeded that of those identified in marine DOM. In particular, aromatic methyl esters occupied  $^1\text{H}$  NMR chemical shifts down to  $\delta_{\text{H}} \sim 4.1$  ppm (section g<sub>3</sub>; Fig. 5) as opposed to  $\delta_{\text{H}} \sim 3.85$  ppm found in marine SPE-DOM FMAX (Fig. 8c; Hertkorn et al., 2013). In addition, aromatic methyl ethers were clearly present in wetland SPE-DOM FCE-L (section g<sub>4</sub>; Fig. 5) but virtually absent in marine SPE-DOM FMAX (Fig. 8c; Hertkorn et al., 2013).

Considerable distinction was observed for HSQC cross peaks which derived from unsaturated protons bound to  $\text{sp}^2$ -hybridized (methine) carbon for FCE-L and FMAX as presented with an overlay of NMR spectra (Fig. S4). Most remarkably, FCE-L showed a much larger abundance and chemical diversity of substituted single aromatic rings across all substitution patterns compared with FMAX, with corresponding methine HSQC cross peaks covering a larger area in general and specific sections in particular. This suggested presence of aromatics with multiple substituted electron-donating functional groups (HSQC cross peaks with  $\delta_{\text{C}} < 120$  ppm; cf. below) which were rare or absent in marine SPE-DOM FMAX. Likely candidates were various plant-derived polyphenols and lignin-derivatives such as polyoxygenated guaiacyl- and syringyl units (HSQC cross peaks d, e, f in Fig. 4; Kim and Ralph, 2010, Martinez et al., 2008, Wen et al., 2013).

Certain substitution patterns could be proposed from reverse increment analysis (Perdue et al., 2007), suggesting presence of up to three oxygen atoms bound to aromatic rings ( $\delta_{\text{C}} < 110$  ppm) as well as similarly high extents of polycarboxylation ( $\delta_{\text{H}} > 8$  ppm). At lower field, HSQC cross peaks of FCE extended further than those of FMAX for both  $^1\text{H}$  and  $^{13}\text{C}$  NMR chemical shifts, suggesting more extensive polycarboxylation in SPE-DOM FCE as well as presence of (more extended) PAH derivatives. Otherwise, abundance and chemical diversity of single and conjugated olefins was larger in SPE-DOM FMAX than FCE-L, suggesting elevated contributions of marine natural products to this region. Overall, HSQC cross peak maxima and specific areas were better resolved in wetland than in marine SPE-DOM. This apparent enhanced molecular diversity of wetland SPE-DOM in comparison with marine SPE-DOM is expected to be genuine for lignin-derived chemical environments and might in part reflect maximum molecular diversity in marine SPE-DOM, resulting in more smooth cross peak distributions in both  $^1\text{H}$  and  $^{13}\text{C}$  NMR frequencies as observed in marine SPE-DOM (see discussion in Hertkorn et al., 2013).

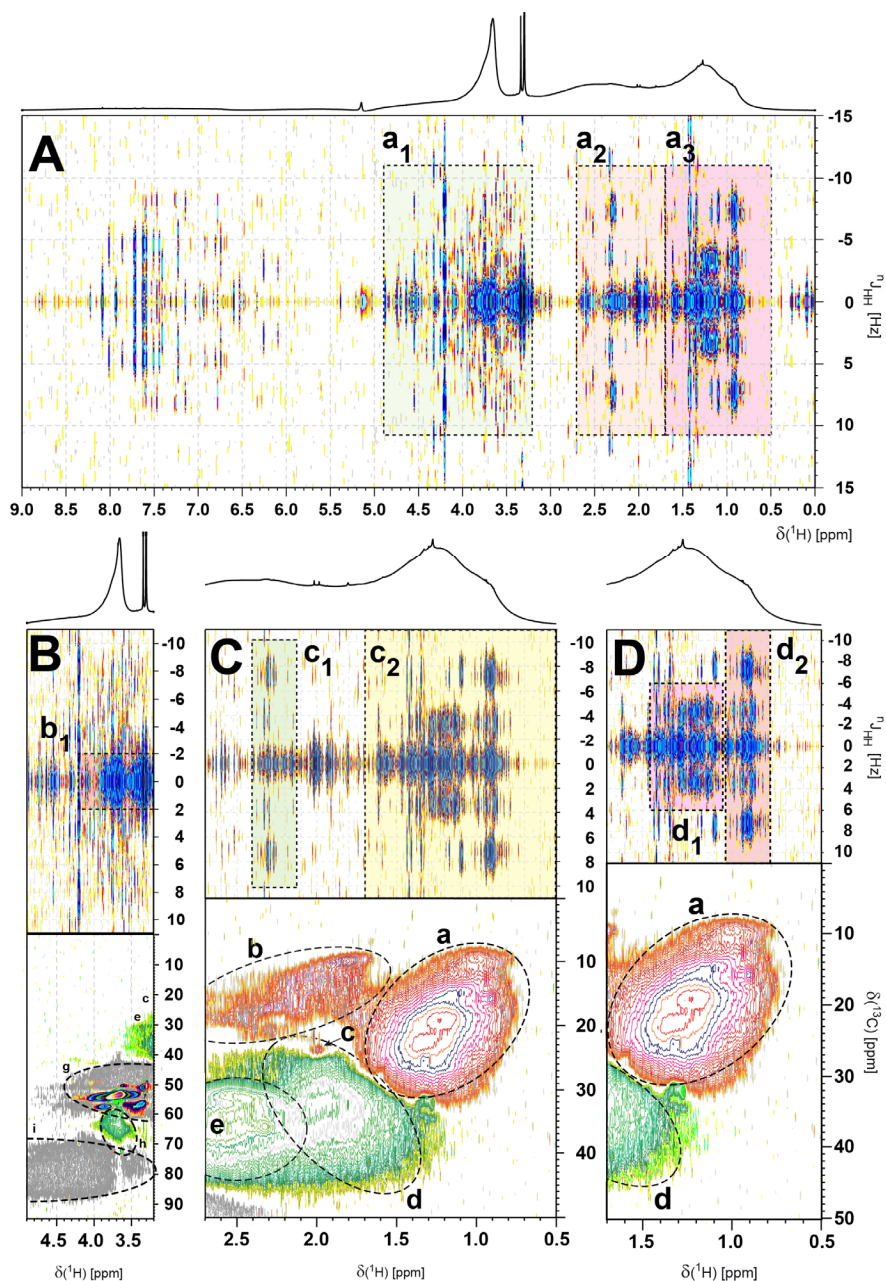


**Figure S6.** Further evaluation of aliphatic spin systems of wetland SPE-DOM FCE-L. Panel A: overall  $^1\text{H}$ ,  $^1\text{H}$  JRES NMR spectrum with sections  $a_1$ ,  $a_2$ ,  $a_3$ , denoting the area of panels B, C, D, which display  $^1\text{H}$  NMR projections along JRES and  $^1\text{H}$ ,  $^{13}\text{C}$  DEPT HSQC NMR spectra (copied from Fig. 5); panel B: section of  $\text{OCH}$  aliphatic units, demonstrating (section  $b_1$ ) presence of intense JRES cross peaks from  $\text{OCH}_3$  groups, with absence of  $J_{\text{HH}}$  splittings; panel C: section of aliphatic  $\text{CCH}$  units, with dominance of  $\text{HOOC-CH}_n\text{-CH}_2\text{-}$  units (triplet  $J_{\text{HH}}$  splitting;  $n = 1, 2$ ) over  $\text{HOOC-CH}_n\text{-CH-}$  units (doublet  $J_{\text{HH}}$  splitting;  $n = 1, 2$ ) shown in section  $c_1$ ; section  $c_2$  indicates panel D; panel D: section of aliphatic  $\text{CCH}$  units, showing a remarkable clustering of  $\text{H}_3\text{C-CH-}$  units at  $\delta_{\text{H}} : 1.0 - 1.4$  ppm, which indicate pronounced aliphatic branching in section  $d_1$  (doublet splitting from  $J_{\text{HH}}$ ), whereas ethyl groups  $\text{H}_3\text{C-CH}_2\text{-}$  dominate the low field section  $\delta_{\text{H}} < 1$  ppm (section  $d_2$ ).

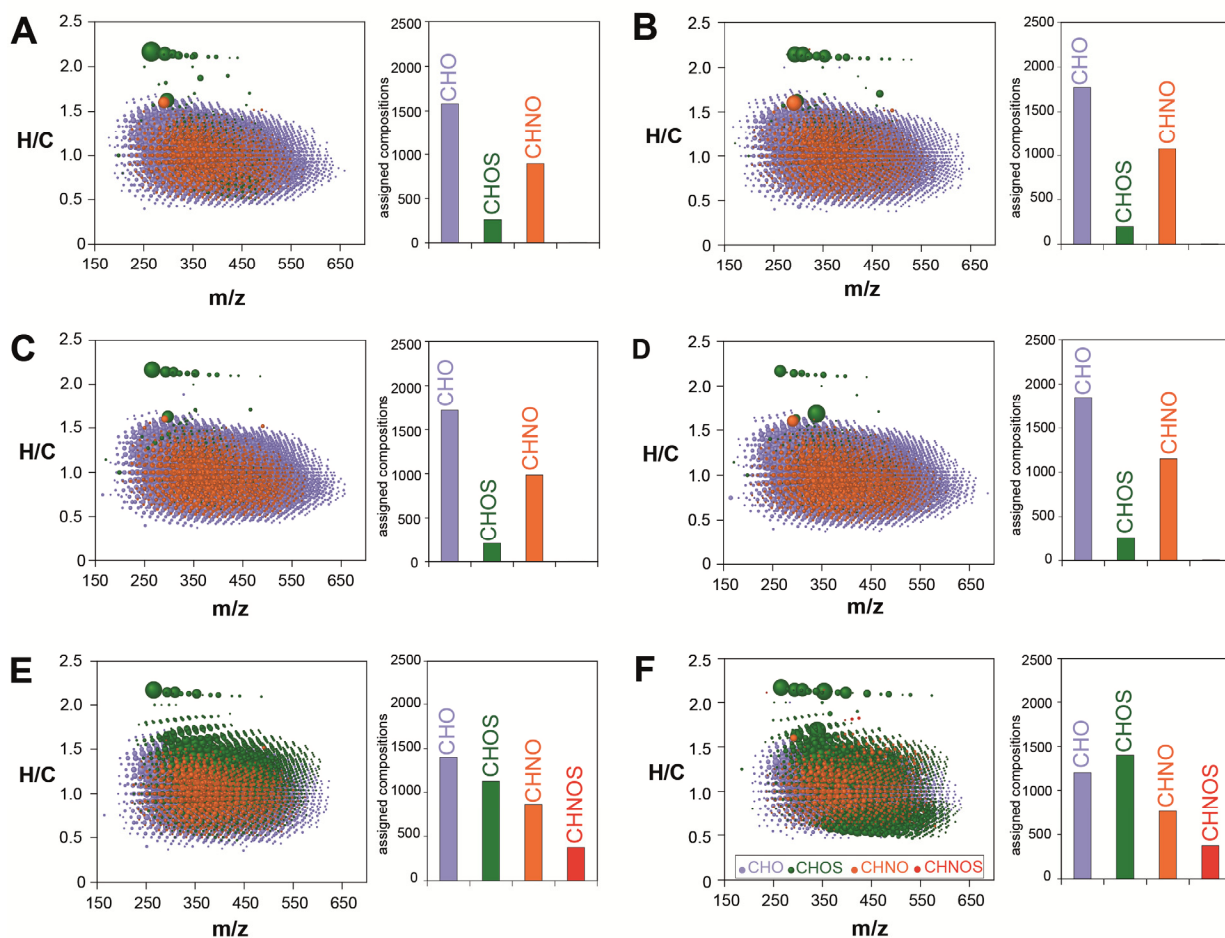


**Figure S7.** Mass edited H/C ratios from negative electrospray 12T FTICR mass spectra of Wetlands SPE-DOM: (A) OKA-L; (B) OKA-S; (C) PAN-L; (D) PAN-S; (E) FCE-L; (F) FCE-S. Inset histograms show the number of assigned molecular compositions. Colour code for elemental compositions bearing combinations of C, H, O, N, and S atoms are defined as follows: blue (CHO), orange (CHNO), green (CHOS) and red (CHNOS). Bubble areas reflect the relative intensities of each mass peak.

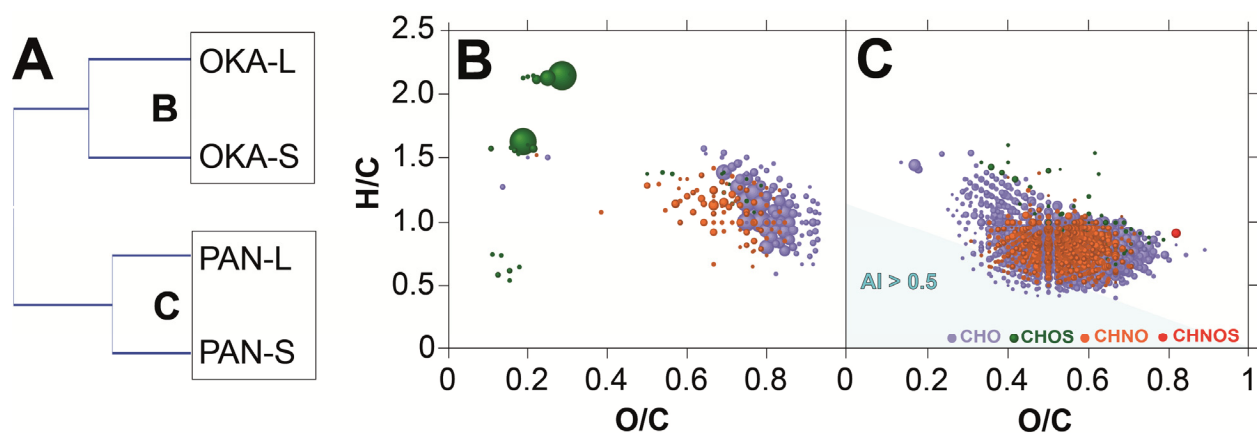


**Figure S8.** Comparative analysis of van Krevelen diagrams derived from negative electrospray 12T FTICR mass spectra derived from four Pantanal and Okavango SPE-OM only. (A) Clustering diagram based on the similarity values between the FTICR mass spectra of these four SPE-DOM; (B) Molecular compositions with rather high abundance in both Okavango SPE-DOM; (C) Molecular compositions with rather high abundance in both Pantanal SPE-DOM, with color code according to molecular series (cf. text). The bright blue triangle denotes aromatic compounds, with aromaticity index  $AI > 0.5$  (Koch and Dittmar, 2006); see Fig. 9 and attendant discussion.

$\delta(^{13}\text{C})$ ppm	220-187	187-167	167-145	145-108	108-90	90-59	59-51	47-0	H/C ratio	O/C ratio
key substructures	$\underline{\text{C}}=\text{O}$	$\underline{\text{C}}\text{OX}$	$\underline{\text{C}}_{\text{ar}}-\text{O}$	$\underline{\text{C}}_{\text{ar}}-\text{C,H}$	$\text{O}_2\underline{\text{C}}\text{H}$	$\text{O}\underline{\text{C}}\text{H}$	$\text{O}\underline{\text{C}}\text{H}_3$	$\text{C}\underline{\text{C}}\text{H}$		
FCE-S	2.5	13.8	2.5	10.3	2.4	14.2	12.6	41.7	<b>1.62</b>	<b>0.64</b>
FCE-L	1.6	13.8	2.2	9.5	0.9	11.9	11.6	48.5	<b>1.70</b>	<b>0.57</b>
OKA-L	2.2	14.8	5.2	17.2	2.4	14.7	7.9	35.6	<b>1.44</b>	<b>0.64</b>
PAN-S	1.8	14.0	5.0	17.2	2.7	14.5	6.9	37.9	<b>1.45</b>	<b>0.62</b>
<b>NMR mixing model</b>	<b><math>\text{C}=\text{O}</math></b>	<b><math>\text{COOH}</math></b>	<b><math>\text{C}_{\text{ar}}-\text{O}</math></b>	<b><math>\text{C}_{\text{ar}}-\text{H}</math></b>	<b><math>\text{O}_2\text{CH}</math></b>	<b><math>\text{OCH}</math></b>	<b><math>\text{OCH}_3</math></b>	<b><math>\text{CH}_2</math></b>		
<b>H/C ratio</b>	<b>0</b>	<b>1</b>	<b>0</b>	<b>1</b>	<b>1</b>	<b>1</b>	<b>3</b>	<b>2</b>		
<b>O/C ratio</b>	<b>1</b>	<b>2</b>	<b>1</b>	<b>0</b>	<b>2</b>	<b>1</b>	<b>1</b>	<b>0</b>		

**Table S1.** (Top):  $^{13}\text{C}$  NMR section integrals (percent of total carbon) and key substructures of wetland SPE-DOM. Bottom: Substructures used for basic NMR-derived reverse mixing model with nominal H/C and O/C ratios given (Hertkorn et al., 2013).

spectrum	Figure	PK	NS	AQ [ms]	D1 [ms]	NE	WDW1	WDW2	PR1	PR2	SPE-DOM [mg]
$^1\text{H}$ NMR	2, S1	5TXI	512-1024	5000	10000	-	-	EM	-	1	3.7 – 9.5 mg
$^{13}\text{C}$ NMR	S3	5D	74496	1000	14000	-	-	EM	-	35	OKA-L 4.7 mg
$^{13}\text{C}$ NMR	S3	5D	44224	1000	14000	-	-	EM	-	35	PAN-S 4.2 mg
$^{13}\text{C}$ NMR	S3	8QCO	23420	1000	19000	-	-	EM	-	35	FCE-L 9.5 mg
$^{13}\text{C}$ NMR	S3	8QCO	3728	1000	19000	-	-	EM	-	35	FCE-S 9.1 mg
$^1\text{H}$ , $^1\text{H}$ TOCSY	4	5TXI	24	1000	2500	1024	QS	EM	2.5	2.5	see caption
$^1\text{H}$ , $^1\text{H}$ TOCSY	4	8QCI	12	1000	2500	1794	QS	EM	2.5	2.5	FCE-S 9.1 mg
$^1\text{H}$ , $^{13}\text{C}$ DEPT HSQC	5	8QCI	320	250	1250	256	QS	EM	2.5	2.5	FCE-S 9.1 mg
$^1\text{H}$ , $^1\text{H}$ JRES	S6	8QCI	3072	1000	500	49	QS	QS	0	0	FCE-S 9.1 mg
$^1\text{H}$ , $^{13}\text{C}$ HSQC	6, S4, S5	8QCI	1600	250	1250	167	QS	EM	4	7.5	FCE-S

**Table S2.** Acquisition parameters of NMR spectra, shown according to figures. PK: probeheads used for acquisition of NMR spectra, 8QCI: cryogenic inverse geometry 5 mm z-gradient  $^1\text{H}/^{13}\text{C}/^{15}\text{N}/^{31}\text{P}$  QCI probe ( $B_0 = 18.8$  T); 8QCO: cryogenic classical geometry 3 mm z-gradient  $^1\text{H}/^{13}\text{C}/^{15}\text{N}/^{31}\text{P}$  probe ( $B_0 = 18.8$  T); 5TXI: cryogenic inverse geometry 5 mm z-gradient  $^1\text{H}$ ,  $^{13}\text{C}$ ,  $^{15}\text{N}$  probe ( $B_0 = 11.7$  T); 5D: cryogenic classical geometry 5 mm z-gradient  $^{13}\text{C}$ ,  $^1\text{H}$  probe ( $B_0 = 11.7$  T); NS: number of scans (for 2D NMR: F2); AQ: acquisition time [ms]; D1: relaxation delay [ms]; NE: number of F1 increments in 2D NMR spectra; WDW1, WDW2: apodization functions in F1/ F2 (EM/GM: line broadening factor [Hz]; QS: shifted square sine bell; SI: sine bell); PR1, PR2: coefficients used for windowing functions WDW1, WDW2, EM/GM are given in [Hz], SI/QS derived functions indicate shift by  $\pi/n$ .

## References:

Hertkorn, N., Harir, M., Koch, B. P., Michalke, B. and Schmitt-Kopplin, P.: High-field NMR spectroscopy and FTICR mass spectrometry: powerful discovery tools for the molecular level characterization of marine dissolved organic matter, *Biogeosciences* **10**, 1583-1624, 2013.

Kim, H., and Ralph, J.: Solution-state 2D NMR of ball-milled plant cell wall gels in DMSO-d(6)/pyridine-d(5), *Org. Biomol. Chem.* **8**, 576-591, 2010.

Martinez, A. T., Rencoret, J., Marques, G., Gutierrez, A., Ibarra D., Jimenez-Barbero, J., and del Rio, J. C.: Monolignol acylation and lignin structure in some nonwoody plants: A 2D NMR study, *Phytochemistry* **69** 2831-2843, 2008.

Perdue, E. M., Hertkorn, N. and Kettrup, A.: Substitution patterns in aromatic rings by increment analysis. Model development and application to natural organic matter, *Analytical Chemistry* **79**, 1010-1021, 2007.

Wen, J.-L., Sun, S.-L., Xue, B.-L., and Sun, R.-C.: Recent Advances in Characterization of Lignin Polymer by Solution-State Nuclear Magnetic Resonance (NMR) Methodology, *Materials* **6**, 359-391, 2013.